An Experimental Methodology for Modeling Surge Protective Devices: An Application to DC SPDs for Electric Vehicle Charging Stations

Thomas E. Tsovilis, *Senior Member, IEEE*, Alexandros Y. Hadjicostas, *Graduate Student Member, IEEE*, Evangelos T. Staikos, *Graduate Student Member, IEEE*, and Georgios D. Peppas, *Senior Member, IEEE*

***Abstract*—This work introduces an experimental methodology for time-domain modeling of low-voltage surge protective devices (SPDs), accounting for their sparkover performance as well as their resistive, inductive, and capacitive behavior. The modeling procedure is demonstrated through an application to a combination type SPD connected to the DC side of electric vehicle charging stations. An equivalent circuit model is developed based on experimental records acquired from applied voltages and currents of a wide frequency range and energy content. The developed lumped-circuit model yields results in very good agreement with experimental data regarding sparkover voltage, residual voltage, and energy absorption of SPDs, as illustrated through ATP-EMTP simulations. The proposed methodology can be an effective tool for surge protection and insulation coordination studies.**

***Index Terms*—ATP-EMTP, fast-front transients, gas discharge tube, slow-front transients, surge protection, varistor.**

I. Introduction

MODERN power grids are intrinsically susceptible to overvoltages as they employ equipment of low insulation levels [1]. The root cause of more than 40% of unexpected failures of electronic equipment is lightning, based on the United States National Fire Protection Association [2]. Thus, extensive research is conducted focusing on the field performance of surge protective devices (SPDs) [3], [4], [5], [6], [7], [8] since the surge protection of low-voltage power grids is of paramount importance for their reliability. Accurate modeling of SPDs is necessary to properly assess the mitigation of overvoltages, evaluate the stress of equipment under protection, and carry out a reasonable risk assessment study against direct and indirect lightning-related surges [9], [10], [11], [12].

Although extensive work has been done for modeling and characterization of surge protective components [13], [14], it is a formidable task to integrate physical models into electromagnetic transients simulation programs. For practical engineering applications, low-voltage surge protective devices are commonly modeled following i) a purely resistive approach based on the voltage-current curves [15], [16], [17] or ii) frequency-dependent models developed for gapless high-voltage surge arresters [18], [19], [20]. The accuracy of these modeling approaches in reproducing the transient performance of low-voltage SPDs for the entire surge current flow duration is questionable [21], [22]. Thus, time-domain modeling of the complex behavior of SPDs in the case of electromagnetic pulses of variable frequencies and energy content is still an open topic.

This work introduces an experimental methodology for modeling low-voltage surge protective devices. The modeling procedure is demonstrated through an application to a commercially available combination type SPD, commonly integrated into converters used in electric vehicle fast chargers operating at 1 kV DC; a preliminary account of this has been provided in [23]. A lumped-circuit model is developed based on standard and non-standard experiments involving i) lightning and switching impulse voltages up to 18 kV, ii) impulse current tests up to 30 kA, and iii) sinusoidal voltages.

The efficiency of the developed model, accounting for the sparkover performance as well as the resistive, inductive and capacitive behavior of the SPD, is validated through a comparison with experimental data regarding sparkover voltage, residual voltage, and energy absorption. The proposed model reproduces the recorded surge performance of the DC SPD under study very accurately, as illustrated through ATP-EMTP simulations; it is found to be more accurate than Pinceti and Giannettoni model [18], which is commonly used in the surge protection industry. The proposed modeling approach can be an effective tool for surge protection and insulation coordination studies [24], [25], [26], especially for emerging DC systems such as battery energy storage systems and electric vehicle charging stations [27], [28], [29], [30].

Manuscript received 21 November 2022; revised 8 May 2023; accepted 31 August 2023. Date of publication 7 September 2023; date of current version 18 January 2024. Paper 2022-PSPC-1276.R1, presented at the 2022 IEEE Industry Applications Society Annual Meeting, Detroit, MI, USA, Oct. 09–14, and approved for publication in the IEEE Transactions on Industry Applications by the Power Systems Protection Committee of the IEEE Industry Applications Society [DOI: 10.1109/IAS54023.2022.9939735]. This work was supported in part by IEEE Industry Applications Society and in part by IEEE Foundation Board (IAS Myron Zucker Student-Faculty Grant Program 2022). *(Corresponding author: Thomas E. Tsovilis)*

Thomas E. Tsovilis, Alexandros Y. Hadjicostas, and Evangelos T. Staikos are with the Electrical and Computer Engineering, Aristotle University of Thessaloniki, 54124 Thessaloniki, Greece (e-mail: tsovilis@auth.gr; chatzikag@ece.auth.gr; evstaikos@ece.auth.gr).

Georgios D. Peppas is with the Research and Development, Raycap, 66100 Drama, Greece (e-mail: peppas@ece.upatras.gr).

Color versions of one or more figures in this article are available at https://doi.org/10.1109/TIA.2023.3312642.

Digital Object Identifier 10.1109/TIA.2023.3312642

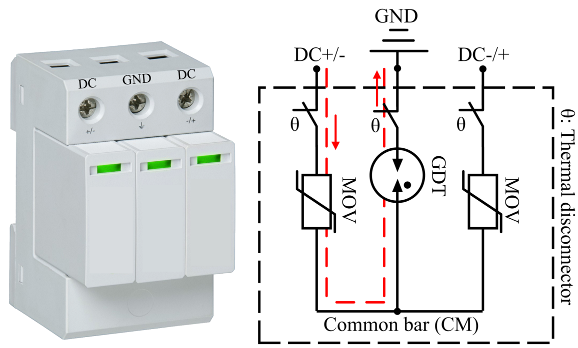

Fig. 1. Schematic diagram of the DIN rail SPD under study.

TABLE I
ELECTRICAL CHARACTERISTICS OF SURGE PROTECTIVE DEVICE

Maximum Continuous Operating Voltage, U_C (kV) [DC+ − DC-]	1.0
Voltage Protection Level, U_p (kV) [DC-GND]	3.2
Impulse Current, I_{imp} (kA), 10/350 µs [DC-GND]	5.0
Nominal Discharge Current, I_n (kA), 8/20 µs [DC-GND]	12.5

II. SURGE PROTECTIVE DEVICE UNDER STUDY

The device under test was a combination type DIN rail surge protective device (SPD) shown in Fig. 1 employing metal-oxide varistors (MOVs) between DC power lines and a gas discharge tube (GDT) connected between a common bar (CM) and ground (GND) that practically eliminates the leakage current to earth. The SPD under study is designed to be connected to charging stations operating at voltages up to 1 kV DC (U_C) and the protection mode under experimental investigation is the power line to ground (DC-GND), designated by the red dashed line in Fig. 1; the basic electrical characteristics of the DC SPD are given in Table I.

III. EXPERIMENTAL ARRANGEMENTS

For the determination of the transient response of the surge protective device under study (Fig. 1), standard lightning LI (1.2/50 μs) and switching SI (250/2500 μs) impulse voltages and standard impulse currents of 8/20 μs and 10/350 μs waveforms were used (Fig. 2(a) and (b)). Taking advantage of the available interchangeable components (Table II) of the High Voltage Laboratory of the Aristotle University of Thessaloniki, the line to ground (DC-GND) protection mode of the SPD was also stressed with non-standard (very fast-front) lightning impulse voltages (0.3/44 μs) and impulse currents (1/130 μs); details on impulse voltage and current waveforms are given in Table III. The impulse currents were recorded by using current transformers (Pearson: 301X, 110), and the residual voltage at SPD terminals was monitored by LeCroy HVP 120 probe (400 MHz) via twisted cables to minimize mutual inductance effects (Fig. 3).

For the determination of the capacitance and the leakage current of the DC SPD, sinusoidal (AC) and DC voltages were applied (Fig. 2(c)) with the aid of a 4.8 kVA AC power supply (Agilent 6843A), and a DC power supply, respectively. The current was measured through the voltage drop, V_{RCur}, across low inductance high-power resistors, R_{Cur}, and a Keithley 196 System DMM current monitor; voltages were monitored by LeCroy HVP120 probe.

For all configurations (Fig. 2) a Tektronix TDS 3064B digital oscilloscope (600 MHz) was employed to record the voltage/current measurements following the UL 1449 [32] and forthcoming IEC 61643-01 [33] standard procedures.

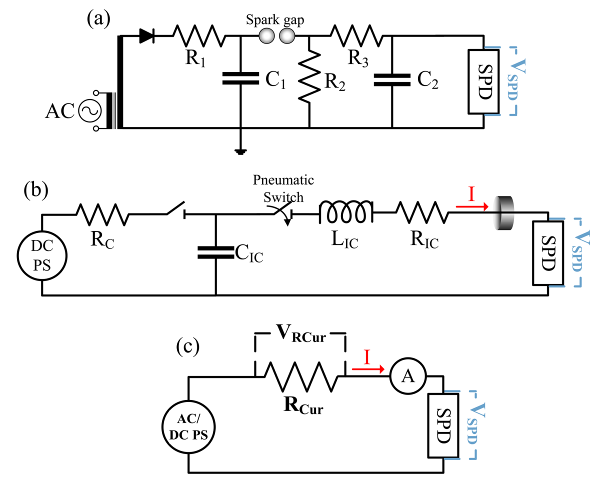

Fig. 2. Experimental arrangement: (a) impulse voltages, (b) impulse currents, and (c) AC/DC voltages.

TABLE II
COMPONENTS OF GENERATORS EMPLOYED IN IMPULSE VOLTAGE AND IMPULSE CURRENT EXPERIMENTS

Impulse Voltage	**1.2/50 µs**	**250/2500 µs**	**0.3/44 µs**
R_1 (MΩ)	10	10	10
C_1 (nF)	25	25	25
R_2 (kΩ)	2.4	98	2.4
C_2 (nF)	1.2	1.2	1.2
R_3 (kΩ)	0.39	57	0.07
Impulse Current	**8/20 µs[1]**	**10/350 µs**	**1/130 µs**
R_C (kΩ)	100	100	100
C_{IC} (µF)	39	269	36
L_{IC} (µH)	1.7	11.5	2.5
R_{IC} (Ω)	0.20	1.9	5

[1] Impulse currents 8/20 µs < 5 kA C_{IC} = 5.3 µF, L_{IC} = 12 µH, R_{IC} = 1.2 Ω

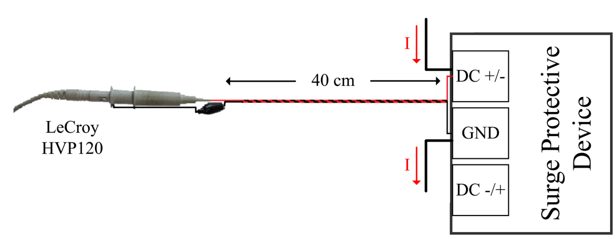

Fig. 3. Residual voltage measurement; adapted from [31].

TABLE III
APPLIED IMPULSE VOLTAGES AND IMPULSE CURRENTS

Impulse Voltage	Time to front $1.67 \times T_{30/90}$ (μs)	Time to crest $T_{0/100}$ (μs)	Time to half t_h (μs)
1.2/50 μs	1.3	2.2	44
250/2500 μs	160	250	2000
0.3/44 μs	0.30	0.55	44
Impulse Current	**Time to front $1.25 \times T_{10/90}$ (μs)**	**Time to crest $T_{0/100}$ (μs)**	**Time to half t_h (μs)**
8/20 μs	7.8	10.6	21.5
10/350 μs	14.5	27.5	405
1/130 μs	1.3	3.0	127

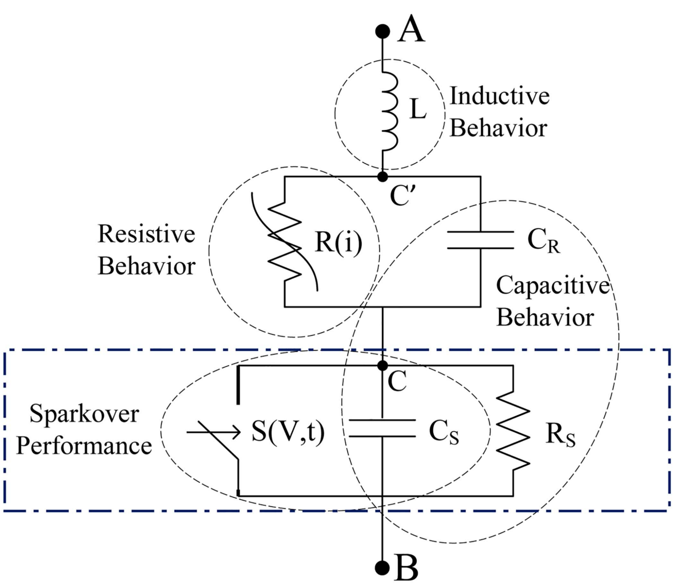

Fig. 4. Proposed model of surge protective devices.

IV. Experimental Methodology for Modeling SPDs

Fig. 4 depicts a generalized equivalent lumped-circuit model (AB) of surge protective devices that comprises of:

a) an intrinsic capacitance, C_S, of the integrated voltage-switching components (spark gaps, gas tubes, etc.) and a switch, *S(V,t)*, that closes when the overvoltage leads to the sparkover of the SPD; if no voltage-switching component is present (voltage-limiting SPD) the rectangular dotted frame in Fig. 4 can be replaced by an ideal short circuit as shown in Fig. 15(a) of Appendix A.

b) a non-linear current-dependent resistance, *R(i)*; the latter is dominated by field-dependent resistivity of the voltage-limiting components (varistors, avalanche diodes, etc.) with an added component of the current-dependent arc resistance of the voltage-switching components; *R(i)* also incorporates the intrinsic resistance of the SPD conductive paths.

c) an inductance, L, that is associated with the intrinsic inductance of SPD conductive paths [34] and the inductive-like behavior of the protective components, especially the effect of holes in surge current conduction via varistors [14], [35].

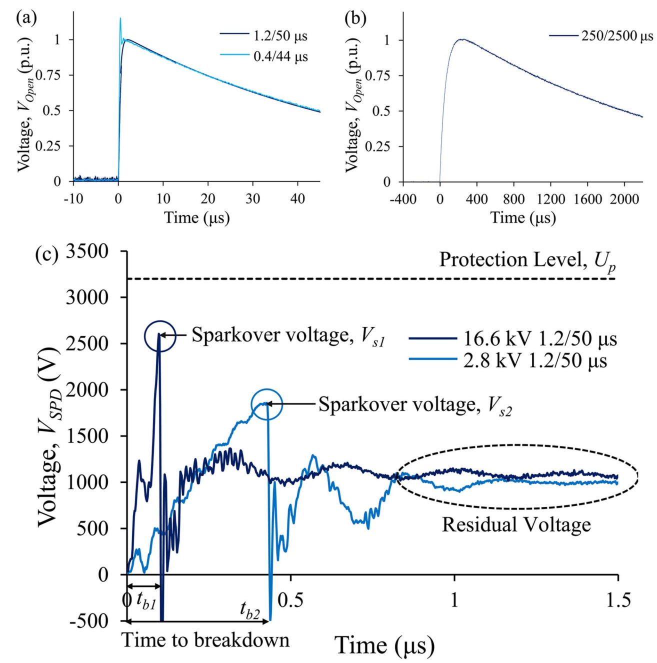

Fig. 5. Impulse voltage experiments: (a) open circuit lightning impulse voltages (p.u,), (b) open circuit switching impulse voltages (p.u,), and (c) sparkover performance of the SPD (DC-GND) for standard lightning impulse voltages.

d) a capacitance, C_R, that represents the intrinsic capacitance of the voltage-limiting components, and a resistance, R_S, that determines the minimal resistive leakage current of the voltage-switching components; if no voltage-limiting component is present (voltage-switching SPDs), C_R can be replaced by an ideal open circuit and the C_S, R_S should be connected in parallel to series connected *R(i)* and *S(V,t)* i.e., between B and C' as shown in Fig. 15(b) of Appendix A.

The voltage-dependent breakdown behavior of the switching components dominates the sparkover performance of the SPD, and the current-dependent resistance of the protective components together with the intrinsic inductive behavior of the SPD dominates its surge performance. The lumped elements of Fig. 4 will be determined through an experimental procedure presented in what follows for the DC SPD under study (Fig. 1).

A. Sparkover Performance

Fig. 5(a) and (b) depict the open circuit (per unit) lightning impulse (1.2/50 μs and 0.3/44 μs) and switching impulse (250/2500 μs) voltages produced by the impulse voltage generator (Fig. 2(a), Tables II and III), respectively. Fig. 5(c) shows typical voltage records at the surge protective device terminals (DC-GND) for applied open-circuit voltages of $\sim$3 kV and $\sim$16 kV, 1.2/50 μs. The voltage at the SPD terminals, V_{SPD}, increases up to the sparkover of the integrated gas discharge tube, GDT (sparkover voltage, V_s). Due to the sudden drop of the SPD impedance, V_{SPD} decreases at the time instant of breakdown (time to breakdown, t_b); the higher the applied voltage, the shorter the time to breakdown and the higher the sparkover voltage (Fig. 5(c)) attaining values always lower than the declared protection level, U_p, of 3.2 kV (Table I). After

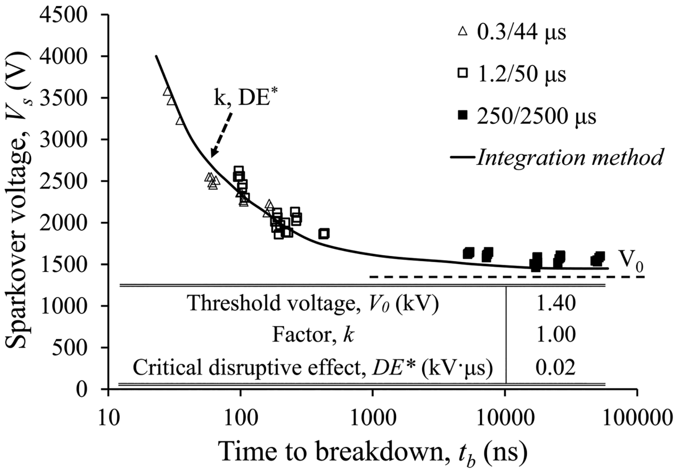

Fig. 6. Sparkover voltage versus time to breakdown of the SPD (DC-GND) for different applied impulse voltages; solid line depicts integration method results acquired under standard impulse voltages (1.2/50 μs and 250/2500 μs).

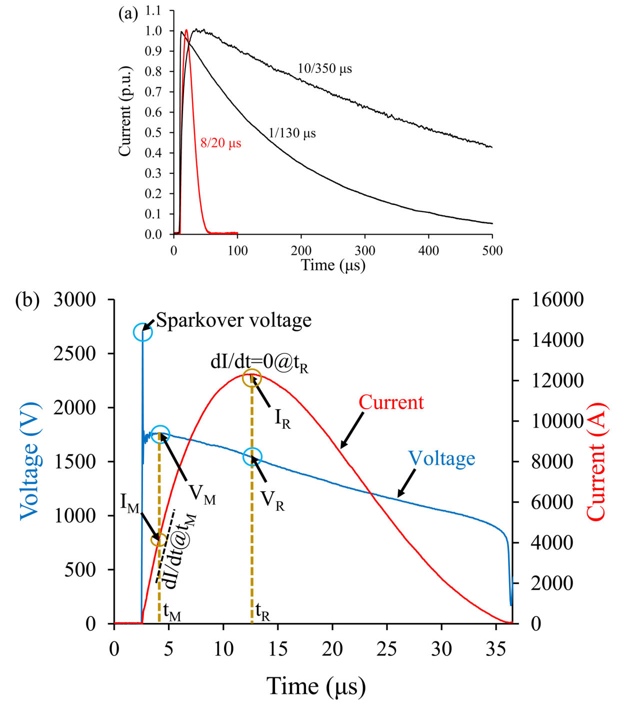

Fig. 7. Impulse current experiments: (a) impulse currents of 8/20 μs, 10/350 μs, 1/130 μs waveform (p.u.) and (b) transient response of the SPD (DC-GND) for nominal discharge current I_n: 12.5 kA, 8/20 μs.

the breakdown of the GDT, a discharge current flows through the series-connected GDT and MOV components (Fig. 1); the residual voltage (∼1 kV) is the sum of the residual voltage of the MOV and the arc voltage of the GDT at the relatively low discharge current of the impulse voltage generator (<60 A).

Fig. 6 depicts the voltage-time data points, V_s-t_b, of the sparkover performance of the SPD under study obtained from lightning and switching impulse voltage tests. As it can be deduced from the slope of the voltage-time curve for time to breakdown lower than 100 ns, there is a significant increase of the SPD sparkover voltage for transients with high voltage derivative (*dV/dt*). This observation stresses the need for an accurate representation of the response time of SPDs integrating voltage-switching components (spark gaps, gas tubes, etc.) as well as the investigation of the protection level of SPDs beyond the standard impulse voltage and current waveforms [36], [22]. The sparkover performance of the SPD under non-standard impulse voltages is modeled by employing the integration method [37], [38] which can be mathematically described as follows:

$$DE = \int_{t_0}^{t} \left(V_{SPD}\left(t\right) - V_0\right)^k dt, \tag{1a}$$

where t (μs) is the elapsed time after the impulse voltage application, t_0 (μs) is the instant when the applied voltage exceeds a threshold voltage, V_0 (kV), k is a factor accounting for the effects of the applied voltage amplitude and waveform [37], [39], and DE (kV^k·μs) is the disruptive effect of the voltage at the SPD terminals, V_{SPD} (kV); breakdown occurs at the time instant, t_b, when DE becomes equal to or higher than the critical disruptive effect DE^*

$$DE = \int_{t_0}^{t_b} \left(V_{SPD}\left(t\right) - V_0\right)^k dt \, \geq DE^*. \tag{1b}$$

The appropriate values for integration method parameters shown in Fig. 6 are selected to minimize the deviation of simulation results with the experimental data points derived from impulse voltage tests representing fast-front [11] and slow-front [40] transients; V_0 is taken from the right side of the curve ($t_b \rightarrow \infty$) and then k, DE^* are computed to fit the experimental data associated with the upturn region of the voltage-time curve.

It is important to note that the sparkover voltage and time to breakdown of the SPD exhibit a statistical behavior since the breakdown of the voltage switching-components is stochastic in nature; an alternative statistical modeling approach treating DE^* employed in (1) as a statistical quantity is presented in Appendix B. For the SPD under study, the stochastic sparkover performance of the integrated GDT depends on several parameters such as electrode morphology, material, and erosion as well as gas mixture composition and pressure [41], [42].

B. Resistive Behavior

Fig. 7(a) depicts the impulse currents (per unit) of standard (8/20 μs and 10/350 μs) and non-standard (1/130 μs) waveform produced by the impulse current generator (Fig. 2(b), Tables II and III), respectively. Fig. 7(b) shows a typical record of the transient response of the SPD (DC-GND) under study when stressed with the nominal discharge current, I_n, of 12.5 kA, 8/20 μs (Table I). It is noteworthy that the voltage spike of ∼2.7 kV, which is the sparkover voltage of the GDT, precedes the maximum residual voltage of the SPD ($V_M \sim 1.8$ kV), and it is associated with the declared protection level of the SPD ($U_p = 3.2$ kV, Table I).

The voltage-current characteristic of the SPD can be obtained by using the residual voltage, V_R, at the peak of the current, I_R, in order to avoid inductive effects on voltage measurement [34] since the current derivative, *dI/dt*, is practically zero at t_R

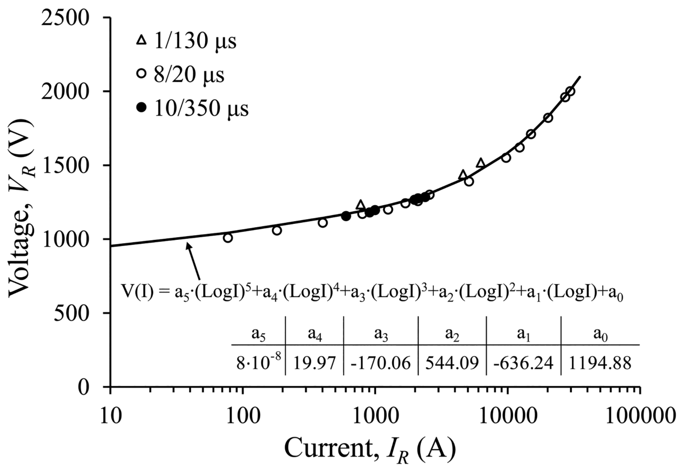

Fig. 8. Voltage-current (V_R, I_R) characteristic curve of the SPD (DC-GND); data points derived from impulse current tests.

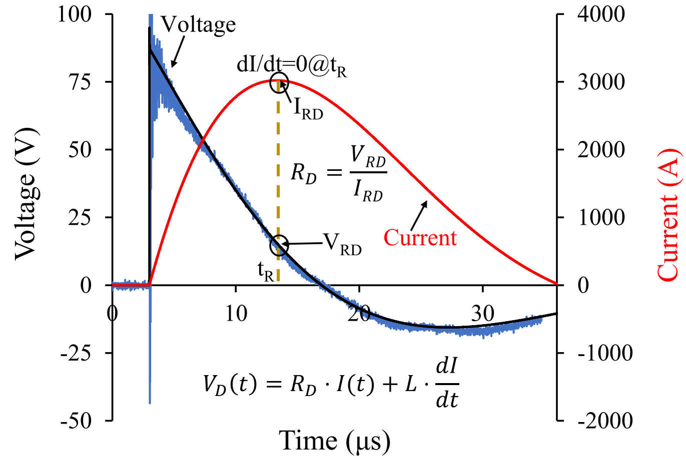

Fig. 9. Surge performance of the dummy SPD under surge current (3 kA, 8/20 μs); L ≈ 130 nH based on (4).

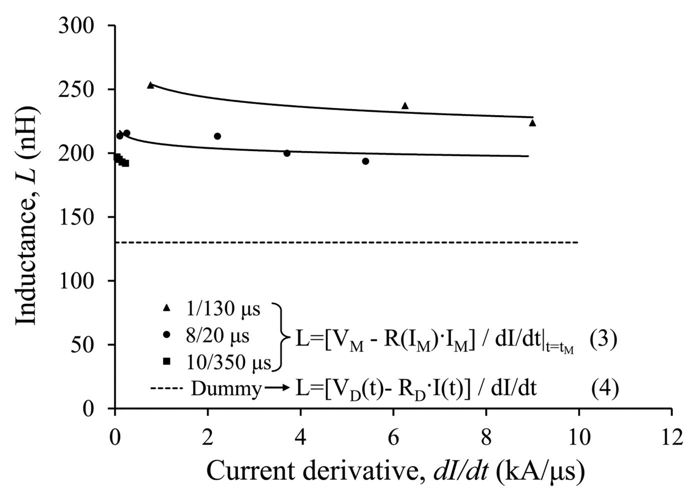

Fig. 10. Equivalent inductance of the SPD.

(Fig. 7(b)). Fig. 8 shows the voltage-current, *V-I*, characteristic curve of the SPD for impulse currents up to 30 kA, that is dominated by the non-linear resistance, *R(I)*, of the MOV together with minor added components of the arc resistance of the GDT and the intrinsic resistance of the SPD conductive path. *R(I)* can be mathematically described as follows:

$$R(I) = V(I)/I = \Big[a_5\,(\log(I))^5 + a_4(\log(I))^4 + a_3(\log(I))^3 + a_2(\log(I))^2 + a_1\log(I) + a_0\Big]\,/\,I. \quad (2)$$

It must be noted that the *V-I* curve depicted in Fig. 8, fits the experimentally derived points (V_R, I_R) at t_R (*dI/dt* = *0*, Fig. 7(b)) and differs from the *V-I* curve that is commonly provided by the SPD manufacturers that employ pairs of the maximum residual voltage, V_M, and current, I_R, that correspond to different time instants (t_M, t_R in Fig. 7(b)). It is important to note that the resistive behavior of the SPD can be described by a single voltage-current (V_R-I_R) curve, that is found to be practically independent of current waveform (Fig. 8); V_R - I_R curve and the associated non-linear resistance, formulated by (2), can be used as a reference for estimating the inductive behavior of the SPD presented in what follows.

C. Inductive Behavior

The fact that the residual voltage of the SPD attains a maximum value, V_M, at t_M before the peak of the current at t_R (Fig. 7(b)) signifies the inductive-like behavior of the SPD, which can be modeled by an equivalent inductance, *L* (AC' in Fig. 4).

The maximum residual voltage of the SPD, V_M, can be well approximated as follows:

$$V_M = R\,(I_M) \cdot I_M + L \cdot dI/dt|_{t\,=\,t_M}, \quad (3)$$

where *R(I)* is given by (2), I_M is the current at the time instant t_M that the maximum residual voltage occurs, *dI/dt* is the current derivative at t_M and *L* is the equivalent inductance. *L* can be evaluated based on (3) since all the other parameters are known through experimental records. Equivalent inductance is associated with the intrinsic inductance of the conductive paths within the structure of the SPD [34], the inductive-like behavior of protective components, and it is contaminated by the mutual inductance of the measuring circuit [31]; the latter can be practically eliminated by employing a voltage measurement setup as shown in Fig. 3.

An alternative procedure for a simplified estimation of *L* is the replacement of the non-linear protective components of the SPD by copper blocks [34]. Such dummy SPD inductance can be measured through high precision impedance analyzers or via the residual voltage, V_D *(t)*, of the SPD during surge current flow, *I(t)* (Fig. 9); the latter can be formulated as:

$$V_D\,(t) = R_D \cdot I\,(t) + L \cdot dI/dt, \quad (4)$$

where R_D is the intrinsic resistance of the dummy SPD.

Fig. 10 shows the inductance, *L*, of the SPD under study (Fig. 1) determined by (3) and (4) for different impulse current experiments. It is obvious that the equivalent inductance depends on i) impulse current waveform and ii) current derivative; it

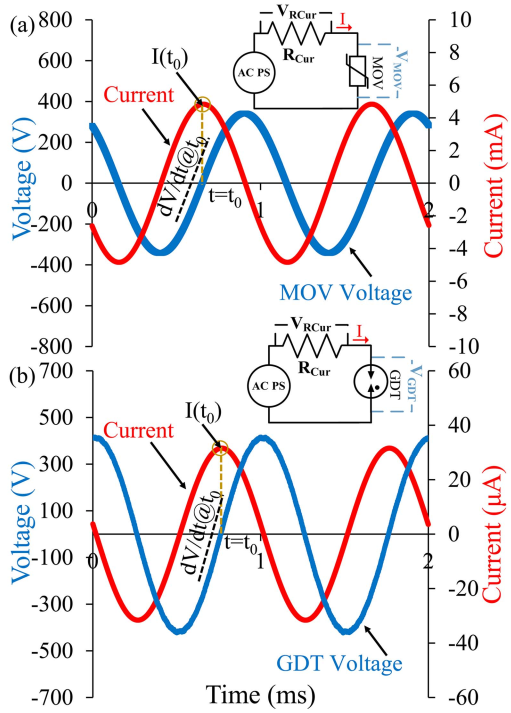

Fig. 11. Capacitive behavior of the SPD components under sinusoidal voltages (AC: 300V rms /1 kHz); (a) MOV and (b) GDT.

is important to note that the dummy SPD analysis underestimates the equivalent inductance of the SPD since it ignores the inductive-like behavior of the surge protective components, especially the transient behavior of MOV for very fast-front surges [35]. A constant L approach, determined at standard impulse currents based on (3), will be shown that provides a satisfactory agreement with experimental results; however, as it can be deduced from Fig. 10 and it is implied in literature [22], [43], [44], the inductive behavior of the SPD is dynamic in nature and L may vary during surge current flow.

D. Capacitive Behavior

The experimental setup of Fig. 2(c) is used to employ sinusoidal voltages to SPD components in order to determine the capacitances at the SPD equivalent circuit model (C_R and C_S in Fig. 4). For the SPD under study an AC voltage of 300V/ 1kHz was applied to the MOV (DC to CM in Fig. 1) and to the GDT (GND to CM in Fig. 1). The current flowing through the MOV or GDT (Fig. 11) at this voltage level (pre-breakdown region) can be described as follows [45]:

$$I(t) = I_C(t) + I_R(t)\,, \tag{5}$$

where $I_C(t)$ is the capacitive component and $I_R(t)$ is the resistive component of the current. Considering that the current at the time instant of zero voltage, t_0, is purely capacitive, the capacitance of the MOV, C_R, or GDT, C_S shown in Fig. 4 can be defined as:

$$C = \frac{I(t_0)}{dV/dt|_{t=t_0}}. \tag{6}$$

A constant C approach is followed, although it is discussed in literature that varistor capacitance C_R may vary with voltage and voltage derivative [45], [46] since the capacitive behavior of the SPD does not significantly affect its surge performance.

The maximum continuous operating voltage of the SPD is applied and the leakage current to the ground is measured (Fig. 2(c)); thus R_S shown in Fig. 4 is estimated (>10 GΩ).

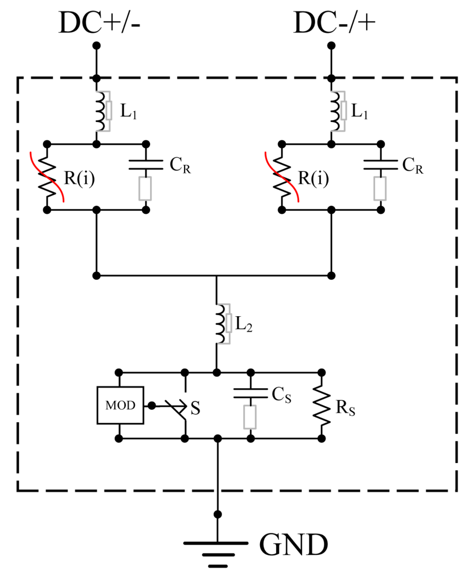

Fig. 12. ATPDraw model of the charging station DC SPD.

TABLE IV
ATP-EMTP MODELING OF THE SPD

Element	Modeling Approach	Input
S	MODEL that controls a TACS type 13 switch	Fig. 6 (Eq. 1 in Section IV.A)
R(i)	Branch nonlinear type 92 resistor	Fig. 8 (Eq. 2 in Section IV.B)
L (L1+L2)	Branch linear inductor, damping factor 7.0	200 (135+65) nH (Eq. 3 in Section IV.C)
C_R	Branch linear capacitor, damping factor 0.15	2.0 nF (Eq. 6 in Section IV.D)
C_S	Branch linear capacitor, damping factor 0.15	12 pF (Eq. 6 in Section IV.D)
R_S	Branch linear resistor	100 GΩ (Section IV.D)

V. ATP-EMTP Simulation Results and Comparison With Experimental Data

A. ATP-EMTP Simulation Model of the SPD

The surge protective device under study (Fig. 1) can be modeled by using the equivalent lumped-element circuit (Fig. 4) that is integrated into ATP-EMTP [47] as shown in Fig. 12; this ATPDraw model reproduces the non-linear performance of the integrated gas discharge tube (GDT) and metal-oxide varistors (MOVs). Modeling details are given in Table IV.

B. Comparison With Experimental Data

The efficiency of the developed ATP-EMTP simulation model (Fig. 12 and Table IV) has been validated through comparison

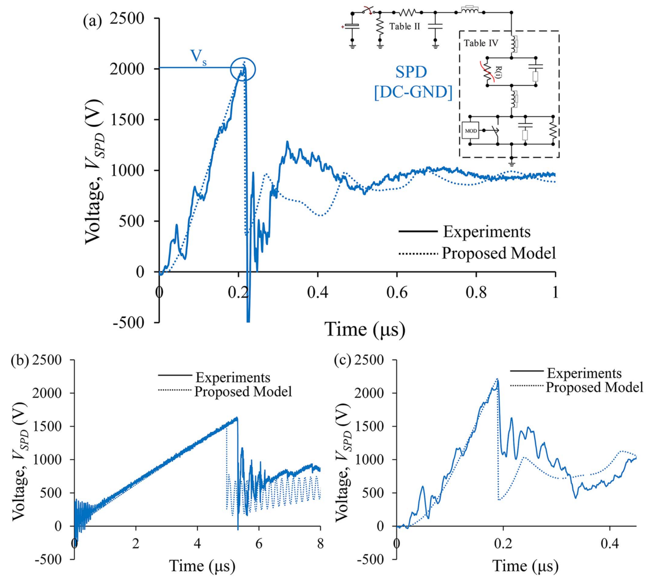

Fig. 13. Voltage at the SPD (DC-GND) under: (a) 6.3 kV, 1.2/50 μs, (b) 18.0 kV, 250/2500 μs, and (c) 2.7 kV, 0.3/44 μs. Measured V_s (V): (a) 2020, (b) 1640, and (c) 2200.

with experimental data. A comparison against the experimentally derived sparkover voltage of the surge protective device (SPD) under study is considered for a wide range of lightning (1.2/50 μs, 0.3/44 μs) and switching impulse voltages (250/2500 μs) up to 18 kV. From Fig. 13 it is evident that there is a good agreement between the simulated and measured sparkover voltages of the SPD. The simulation error was generally less than 10% (max 14.8%) as detailed in Table V for 3 impulses per voltage level; the simulation accuracy is satisfactory when considering the expected spread of the sparkover voltage of the integrated GDT [41], which is typically declared within 20% by GDT manufacturers [48]. Nevertheless, to further improve the accuracy of the predictions of the proposed deterministic modeling approach on the sparkover performance of SPDs, an alternative statistical method is proposed in Appendix B; this method yields a range of sparkover voltage instead of a fixed value (Fig. 18).

Fig. 14 shows simulation results together with voltage and current records from impulse current tests. The computed residual voltage of the SPD (V_M, V_R as defined in Fig. 7(b)) with the proposed model is in very good agreement with the experimental data (simulation error $< 6\%$) derived from impulse current tests up to 30 kA, 8/20 μs, 2.5 kA, 10/350 μs and 6.2 kA, 1/130 μs (Table VI); these upper limits were about 50% of the surges producing irreversible degradation to SPD components. On the contrary, the agreement of the Pinceti and Giannettoni (P&G) model [18] (details in Appendix A), commonly used in surge protection industry, is not always adequate, besides the use of 2 non-linear resistive elements, especially for non-standard current waveforms and peak values afar the reference level of 10 kA; the latter is understandable since the P&G model has been developed for high voltage surge arrester and a lot of technical data required as inputs are not provided by manufacturers of low-voltage SPDs. A necessary modification of the original

TABLE V
SIMULATION ERRORS IN SPARKOVER VOLTAGE OF THE SURGE PROTECTIVE DEVICE

	Open circuit voltage, U_{open} (kV)	Absolute error* in V_s (%) Applied Impulse 1	2	3
1.2/50 μs	2.8	6.20	6.58	5.85
	4.6	8.43	3.49	5.38
	5.5	0.07	7.37	7.68
	6.3	11.8	6.55	2.81
	7.1	3.51	0.68	6.10
	13.8	2.03	7.30	0.30
	16.6	0.08	0.46	2.38
	Max:	**11.8**		
	Average:	**4.53**		
250/2500 μs	2.7	6.49	5.88	7.10
	4.0	4.47	8.10	7.34
	6.0	5.00	2.92	3.88
	13.0	7.02	5.25	7.59
	18.0	7.68	6.54	7.12
	Max:	**8.10**		
	Average:	**6.16**		
0.3/44 μs	2.7	4.17	0.42	0.91
	6.0	7.37	7.73	12.0
	11.2	14.7	12.1	13.4
	15.0	2.31	9.89	14.8
	18.0	12.1	14.2	2.90
	Max:	**14.8**		
	Average:	**8.60**		

$$* \textit{Absolute error} = \frac{|\textit{Measurement} - \textit{Simulation}|}{|\textit{Measurement}|} \cdot 100\%$$

TABLE VI
SIMULATION ERRORS IN RESIDUAL VOLTAGE AND ENERGY ABSORPTION OF THE SURGE PROTECTIVE DEVICE

Waveform	Current (kA)	Proposed model Absolute error* in V_M (%)	V_R (%)	E (%)	Adapted P&G model Absolute error* in V_M (%)	V_R (%)	E (%)
8/20 μs	1.25	0.87	0.80	3.03	12.7	9.37	14.0
	2.50	1.22	1.08	0.58	13.8	6.11	9.06
	5.00	3.21	0.29	1.53	9.57	6.99	9.44
	12.5	2.46	0.74	0.29	3.99	4.63	2.74
	20.0	0.69	2.97	1.62	1.59	1.46	2.63
	30.0	0.80	2.68	1.01	6.16	1.52	7.53
	Max:	**3.21**	**2.97**	**3.03**	**13.8**	**9.37**	**14.0**
	Average:	**1.54**	**1.43**	**1.34**	**7.97**	**5.01**	**7.57**
10/350 μs	0.50	4.45	2.80	2.93	6.19	7.99	14.6
	1.00	2.44	1.80	4.77	6.71	6.70	12.5
	1.50	3.51	0.52	0.02	5.99	7.00	9.19
	2.00	2.34	1.65	3.75	8.23	5.85	11.8
	2.50	1.29	0.76	0.53	8.45	4.47	7.40
	Max:	**4.45**	**2.80**	**4.77**	**8.45**	**7.99**	**14.6**
	Average:	**2.81**	**1.51**	**2.40**	**7.11**	**6.40**	**11.1**
1/130 μs	0.80	1.44	5.42	2.84	11.5	4.03	14.2
	4.60	4.47	4.27	2.56	0.61	12.3	8.75
	6.20	4.34	5.36	1.28	6.17	9.93	7.14
	Max:	**4.47**	**5.42**	**2.84**	**11.5**	**12.3**	**14.2**
	Average:	**3.42**	**5.02**	**2.23**	**6.09**	**8.75**	**10.0**

$$* \textit{Absolute error} = \frac{|\textit{Measurement} - \textit{Simulation}|}{|\textit{Measurement}|} \cdot 100\%$$

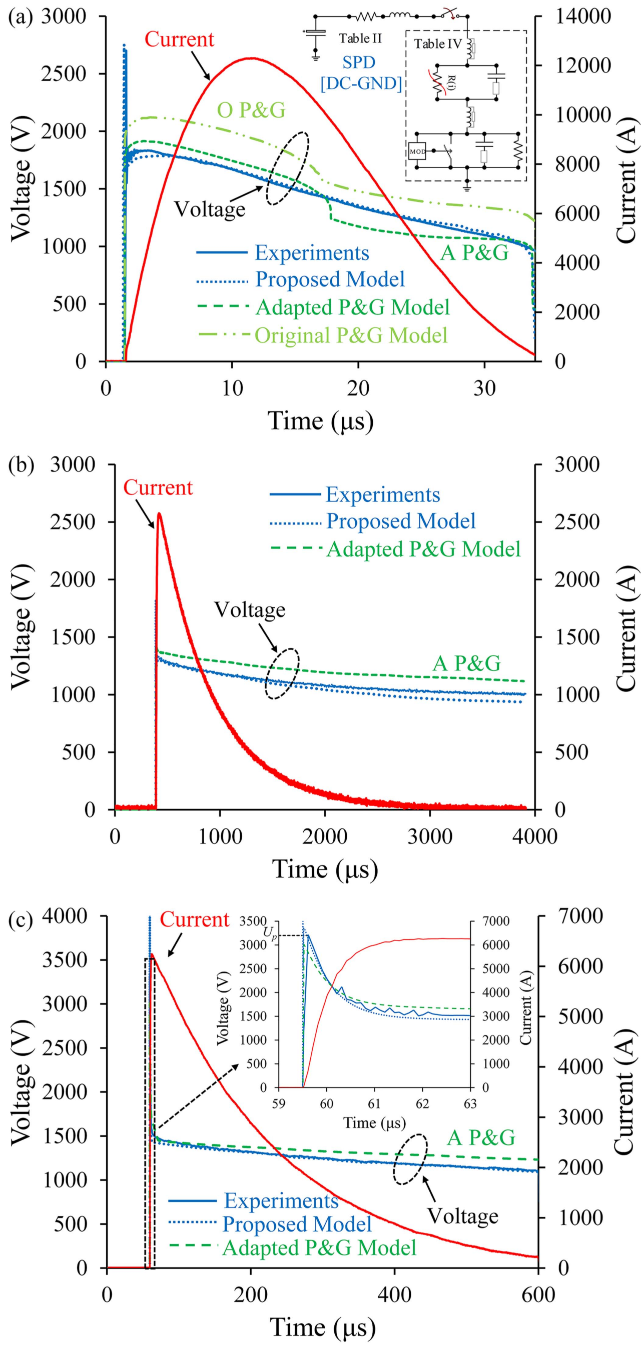

Fig. 14. Voltage and current at the SPD (DC-GND): (a) I_n:12.5 kA, 8/20, (b) I_{imp}: 2.5 kA, 10/350 μs, and (c) 6.2 kA, 1/130 μs. Measured data [V_M (V), V_R (V), E (J)]: (a) (1830, 1620, 346), (b) (1320, 1313, 1702), and (c) (3220, 1518, 1412).

P&G model is introduced by the authors to yield simulation results with acceptable errors (<15%) as shown in Fig. 14(a). Model has been adapted as follows: i) non-linear resistances A0, A1 were calculated based on the residual voltage V_R, instead of V_M, at 10 kA, 8/20 μs ii) L0, L1 were computed based on resistive residual voltage V_R at 10 kA 8/20 μs and V_M at 10 kA 1/T2 μs instead of using V_M values at 10 kA, 8/20 μs and 1/T2 μs; an application is shown in Appendix A.

It is noteworthy that the proposed model predicts the development of a maximum residual voltage beyond the protection level of the SPD for ~6 kA, 1/130 μs, whereas the adapted P&G model underestimates (6%) the overshoot of the residual voltage (inset graph Fig. 14(c), measured $V_M = 3.22$ kV); this overshoot is important when considering the very fast-front transient performance of SPDs in cases such as subsequent lightning strokes [41] and nuclear electromagnetic pulses [49].

In order to evaluate the efficiency of the developed model to reproduce the SPD transient behavior for the complete surge current duration an additional comparison is made for the energy absorption, E, of the SPD defined as:

$$E = \int V_{SPD}\left(t\right) \cdot I\left(t\right) dt, \tag{7}$$

where $V_{SPD}(t)$ is the voltage across the SPD during surge current flow, $I(t)$. The proposed model yields results in excellent agreement with the recorded energy absorption, that is one of the main parameters determining the SPD failure probability, with simulation errors generally lower than 3% (max 4.8%) whereas the adapted P&G model computations are associated with errors up to 15% (original model yields errors up to 25%). These results are very encouraging when considering that the measurement error of voltage and current records is within 3% and that voltage-current characteristics of metal-oxide varistors of the same type may vary up to 10% [50].

VI. Conclusion

A novel experimental methodology has been introduced for modeling low-voltage surge protective devices (SPDs). An application has been made to a combination type SPD connected to the DC side of electric vehicle charging stations and an equivalent lumped-element circuit model has been developed. The experimental investigation of the transient performance of the DC SPD for a wide range of impulse voltage (2.5 kV–18 kV) and impulse current (0.5 kA – 30 kA) tests has shown that:

- The sparkover performance of the SPDs can be evaluated through voltage-time (V_s-t_b) curves derived from impulse voltage tests. The integration method proved an efficient tool for modeling the sparkover performance of the SPD against overvoltages with time to front in the range of ~0.3–250 μs and time to half of ~40–2000 μs.
- The resistive behavior of the SPDs can be described by a single voltage-current (V_R-I_R) characteristic curve, derived from residual voltage measurements at the time instant of the peak of the impulse current (zero current derivative). The voltage-current curve is found to be practically independent of the surge current waveform unlike the *V-I* curves provided by SPD manufacturers that employ pairs of the maximum residual voltage and peak current that correspond to different time instants.
- The maximum residual voltage of SPDs during surge currents is associated with the intrinsic inductance of SPD conductive paths and the inductive-like behavior of the integrated protective components. The inductive behavior of the SPD can be modeled through a lumped inductance that is found to be dynamic in nature. A constant inductance estimated at nominal discharge current can be adopted as a simplified approach for modeling the overshoot of the residual voltage at the wavefront without compromising

the accuracy at the wave-tail for a wide range of surge currents with time to front between ~1–30 μs and time to half between ~20–400 μs.
- The capacitive behavior of the SPD, that does not significantly affect its transient behavior, can be evaluated at the time instant of zero voltage under low frequency tests.

The developed model has been incorporated in ATP-EMTP; a comparison of simulation results with experimental data has shown that:
- The proposed model yields satisfactory results for standard and non-standard (very fast-front) impulse voltages with simulation errors less than 15% in the SPDs sparkover voltage. The integration method-based approach predicts satisfactorily the SPD performance for fast-front and slow-front overvoltages; a statistical modeling approach is needed for further improvement in the prediction of the sparkover performance of SPDs.
- The proposed model yields excellent results for standard and non-standard (very fast-front) impulse currents with simulation errors generally less than 5% in the SPDs residual voltage and the associated energy absorption. The inclusion of a series inductance in series with a single current-dependent resistance, masking the capacitive behavior of the SPD, yields very good results in modeling the transient behavior of the SPD for a wide range of surge currents. The Pinceti & Giannettoni model, besides its frequency-dependent behavior, is less accurate on modeling low-voltage SPDs, especially under non-standard impulse currents; a necessary modification is proposed for model implementation to low-voltage SPDs so as to yield simulation results with acceptable errors.

APPENDIX A
EQUIVALENT CIRCUIT MODELS

Equivalent circuit models of voltage-limiting and voltage-switching SPDs are shown in Fig. 15.

Pinceti and Giannettoni model [18] employed at AC branch of Fig. 4 (DC to CM in Fig. 1). Original model details, and values as adapted by the authors for low-voltage SPDs are given in Fig. 16.

APPENDIX B
STATISTICAL APPROACH FOR MODELING THE SPARKOVER PERFORMANCE

The integration method, presented in Section IV-A, is inherently deterministic with simulation errors up to 15%; however, by treating the critical disruptive effect DE^* as a statistical quantity rather than a fixed value, the stochastic sparkover performance of the SPDs can be modeled yielding a range of sparkover voltage under the same overvoltage conditions. As an illustrative example for the DC SPD under study, the following equation defines the criterion of breakdown at time instant ($t = t_b$) that DE becomes equal to or higher than the critical disruptive effect DE^*

$$DE = \int_{t_0}^{t_b} (V_{SPD}(t) - V_0)\, dt \geq 0.005 \cdot (1 + 6 \cdot r) = DE^* \quad (8)$$

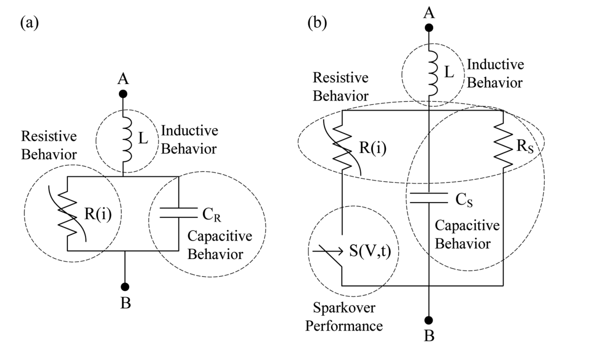

Fig. 15. Proposed model of surge protective devices. (a) Voltage-limiting SPD and (b) voltage-switching SPD.

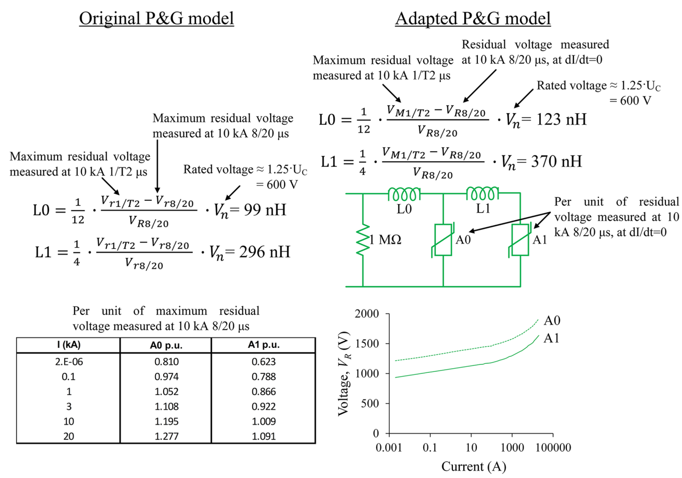

I (kA)	A0 p.u.	A1 p.u.
2.E-06	0.810	0.623
0.1	0.974	0.788
1	1.052	0.866
3	1.108	0.922
10	1.195	1.009
20	1.277	1.091

Fig. 16. Original and adapted Pinceti and Giannettoni (P&G) model [18].

```
INIT
DE*:=0.005*(1+6*random())
```

Fig. 17. Code in MODELS language for determining DE^*.

where r takes random values between 0 and 1 for each simulation run, t (μs) is the elapsed time after the impulse voltage application, t_0(μs) is the instant when the applied voltage exceeds a threshold voltage, V_0 (kV), t_b is the time to breakdown, DE (kV·μs) is the disruptive effect of the voltage at the SPD terminals, V_{SPD} (kV); DE^* is uniformly distributed between 0.005 and 0.035 kV·μs based on (8). Such a statistical variation of DE^* can be integrated into ATP-EMTP environment through MODELS language [51] as shown in Fig. 17.

Employing (8) in ATP-EMTP (Fig. 17) for multiple simulation runs, a range of sparkover voltage is obtained even under the same overvoltage conditions; this is shown in Fig. 18, which depicts the borders of the voltage-time variation corresponding to the range of DE^* (0.005–0.035 kV·μs). As an illustrative example, Fig. 19 shows the SPD sparkover simulation results under 11.2 kV, 0.3/44 μs for the mean value of DE^* (0.02 kV·μs) employed in the conventional integration method that yields error on sparkover voltage of ~15% and the value of 0.011 kV·μs that lies within the statistical range of DE^* that accurately predicts the sparkover voltage (error $<$ 1%).

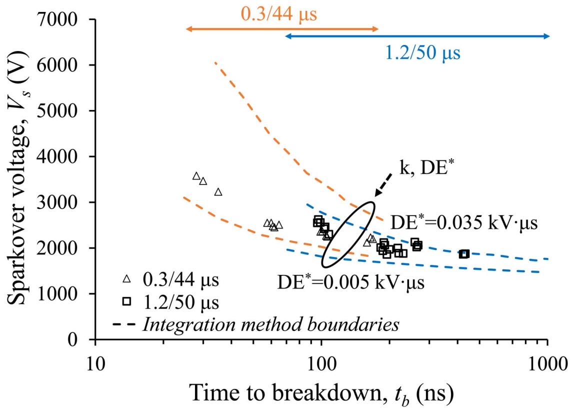

Fig. 18. Sparkover voltage versus time to breakdown under fast-front transients based on the statistical modeling approach.

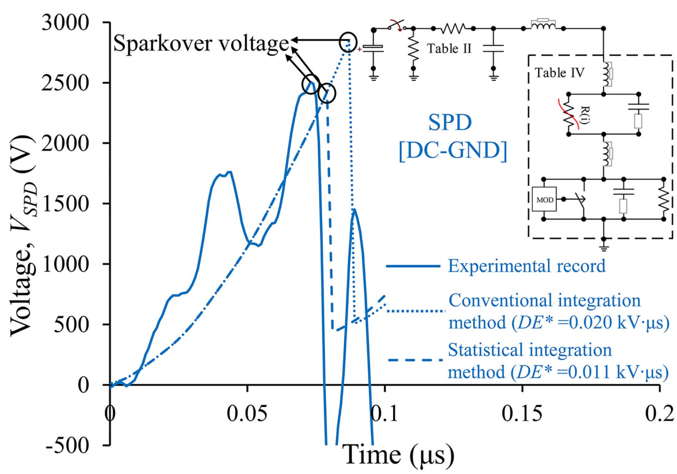

Fig. 19. Sparkover performance of the SPD under study for different DE^* values; comparison with experimentally derived sparkover performance under 11.2 kV, 0.3/44 μs.

Acknowledgment

Prof. Thomas E. Tsovilis and Dr. George D. Peppas wish to thank Mr. Thomas Kohushölter, Head of VDE Testing and Certification Institute in Berlin, for their fruitful discussions on the surge performance of DC surge protective devices. The authors would like to thank Prof. Pantelis N. Mikropoulos and Mr. Pavlos K. Samaras for their kind advice and support on the experimental part of this work. The publication of the article in OA mode was financially supported by HEAL-Link.

References

[1] A. Rousseau, *Surge Protection for Low Voltage Systems*. London, U.K.: IET Energy Eng., 2021.

[2] E. Davis, N. Kooiman, and K. Viswanathan, *Data Assessment for Electrical Surge Protective Devices*. Quincy, MA, USA: Fire Protection Res. Found., 2014.

[3] F. D. Martzloff, "Matching surge protective devices to their environment," *IEEE Trans. Ind. Appl.*, vol. IA-21, no. 1, pp. 99–106, Jan. 1985.

[4] K. W. Eilers, M. Wingate, and E. Pham, "Application and safety issues for transient voltage surge suppressors," *IEEE Trans. Ind. Appl.*, vol. 36, no. 6, pp. 1734–1740, Nov./Dec. 2000.

[5] K. Samaras, C. Sandberg, C. J. Salmas, and A. Koulaxouzidis, "Electrical surge-protection devices for industrial facilities—A tutorial review," *IEEE Trans. Ind. Appl.*, vol. 43, no. 1, pp. 150–161, Jan./Feb. 2007.

[6] D. T. Khanmiri, R. Ball, and B. Lehman, "Degradation effects on energy absorption capability and time to failure of low voltage metal oxide varistors," *IEEE Trans. Power Del.*, vol. 32, no. 5, pp. 2272–2280, Oct. 2017.

[7] S. Chen, Y. Zhang, M. Zhou, X. Yan, W. Lu, and Y. Zhang, "Influence on low-voltage surge protective devices of overhead distribution lines due to nearby return strokes," *IEEE Trans. Power Del.*, vol. 33, no. 3, pp. 1099–1106, Jun. 2018.

[8] K. Yamamoto and Y. Mendez, "Renewable energy systems-photovoltaic systems," in *Lightning Interaction With Power Systems - Volume 2: Applications*, A. Piantini, Ed. London, U.K.: IET Energy Eng., Jan. 2020, pp. 343–370.

[9] K.-C. Lai, W.-J. Lee, and W. V. Jackson, "Testing and selecting surge suppressors for low-voltage AC circuits," *IEEE Trans. Ind. Appl.*, vol. 26, no. 6, pp. 976–982, Nov./Dec. 1990.

[10] M. O. Durham, K. D. Durham, and R. A. Durham, "TVSS designs," *IEEE Ind. Appl. Mag.*, vol. 8, no. 5, pp. 31–36, Sep./Oct. 2002.

[11] T. R. Brinner and R. A. Durham, "Transient-voltage aspects of grounding," *IEEE Trans. Ind. Appl.*, vol. 46, no. 5, pp. 1796–1804, Sep./Oct. 2010.

[12] *Protection Against Lightning - Part 4: Electrical and Electronic Systems Within Structures*, Standard IEC 62305-4:2010, 2010. [Online]. Available: https://webstore.iec.ch/publication/6796

[13] T. Runge, T. H. Kopp, and M. Kurrat, "Investigation methods and techniques for plasma characterisation in a spark gap model at surge currents - A review," in *Proc. IEEE 34th Int. Conf. Lightning Protection*, 2018, pp. 1–6.

[14] F. Greuter, "ZnO Varistors: From grain boundaries to power applications," in *Oxide Electronics*, A. Ray, Ed. Hoboken, NJ, USA: Wiley, 2021, pp. 157–234.

[15] Z. Topcagic, M. Mlakar, and T. E. Tsovilis, "Electrothermal and overload performance of metal-oxide varistors," *IEEE Trans. Power Del.*, vol. 35, no. 3, pp. 1180–1188, Jun. 2020.

[16] T. Tanaka, R. Tsuge, Y. Baba, Y. Tsujimoto, and N. Tsukamoto, "An approximate mathematical expression for nonlinear resistive properties of metal oxide varistor elements for FDTD simulations," *IEEE Trans. Electromagn. Compat.*, vol. 62, no. 6, pp. 2638–2642, Dec. 2020.

[17] Q. Zhou, H. Yang, X. Huang, M. Wang, and X. Ren, "Numerical modelling of MOV with Voronoi network and finite element method," *IET High Voltage*, vol. 6, pp. 711–717, 2021.

[18] P. Pinceti and M. Giannettoni, "A simplified model for zinc oxide surge arresters," *IEEE Trans. Power Del.*, vol. 14, no. 2, pp. 393–398, Apr. 1999.

[19] R. Kannadasan and P. Valsalal, "Modelling and validation of metal oxide surge arrester for very fast transients," *IET High Voltage*, vol. 3, no. 2, pp. 147–153, Jun. 2018.

[20] V. S. Brito, G. R. S. Lira, E. G. Costa, and M. J. A. Maia, "A wide-range model for metal-oxide surge arrester," *IEEE Trans. Power Del.*, vol. 33, no. 1, pp. 102–109, Feb. 2018.

[21] A. Pirih and A. Pregelj, "Contribution to mathematical modelling of metal oxide surge arresters based on exact analysis of parasitic inductive influences," in *Proc. 40th Int. Conf.*, 2004, pp. 225–230.

[22] R. Montaño, M. Edirisinghe, V. Cooray, and F. Roman, "Behavior of low-voltage surge protective devices under high-current derivative impulses," *IEEE Trans. Power Del.*, vol. 22, no. 4, pp. 2185–2190, Oct. 2007.

[23] T. E. Tsovilis, A. Y. Hadjicostas, E. T. Staikos, and G. D. Peppas, "Modeling the transient behavior of surge protective devices connected to the DC side of electric vehicle charging stations," in *Proc. IEEE Ind. Appl. Soc. Annu. Meeting*, 2022, pp. 1–6.

[24] J.-S. Lai and F. D. Martzloff, "Coordinating cascaded surge protection devices: High-low versus low-high," *IEEE Trans. Ind. Appl.*, vol. 29, no. 4, pp. 680–687, Jul./Aug. 1993.

[25] Y. Zhang, H. Chen, Y. Du, Z. Li, and Y. Wu, "Lightning transient analysis of main and submain circuits in commercial buildings using PEEC Method," *IEEE Trans. Ind. Appl.*, vol. 56, no. 1, pp. 106–116, Jan./Feb. 2020.

[26] E. T. Staikos, G. D. Peppas, and T. E. Tsovilis, "Wide frequency response of varistors and coordination with transient voltage suppression diodes," *IEEE Trans. Power Del.*, vol. 38, no. 1, pp. 453–462, Feb. 2023.

[27] J. Birkl, T. Böhm, and E. Shulzhenko, "Earthing systems for charging infrastructures –impact in case of lightning incidents," in *Proc. 36th Int. Conf. Lightning Protection*, 2022, pp. 318–326.

[28] B. Wang, P. Dehghanian, S. Wang, and M. Mitolo, "Electrical safety considerations in large-scale electric vehicle charging stations," *IEEE Trans. Ind. Appl.*, vol. 55, no. 6, pp. 6603–6612, Nov./Dec. 2019.

[29] F. Teng, Z. Ding, Z. Hu, and P. Sarikprueck, “Technical review on advanced approaches for electric vehicle charging demand management, part i: Applications in electric power market and renewable energy integration,” *IEEE Trans. Ind. Appl.*, vol. 56, no. 5, pp. 5684–5694, Sep./Oct. 2020.

[30] N. S. Kelepouris, A. I. Nousdilis, A. S. Bouhouras, and G. C. Christoforidis, “Cost-effective hybrid PV-battery systems in buildings under demand side management application,” *IEEE Trans. Ind. Appl.*, vol. 58, no. 5, pp. 6519–6528, Sep./Oct. 2022.

[31] OSM/IN 288 for EN 61643 series + EN 50539 series, “General instruction for residual voltage measurements,” Decided 2018 (meeting 28). [Online]. Available: https://www.etics.org/doc/doc_15755_main1_OSM-IN%20288.pdf

[32] *Standard for Safety, Surge Protective Devices, SB Supplement: Direct Current (DC) SPDs*, Standard UL 1449, Ed. 5, 2021.

[33] *Low-Voltage Surge Protective Devices - Part 01: General Requirements and Test Methods*, Standard IEC 61643-01 ED1, to be published, 2024.

[34] T. E. Tsovilis, “Critical insight into performance requirements and test methods for surge protective devices connected to low-voltage power systems,” *IEEE Trans. Power Del.*, vol. 36, no. 5, pp. 3055–3064, Oct. 2021.

[35] P. F. Tua, M. Rossinelli, and F. Greuter, “Transient response of electrically active grain boundaries in polycrystalline semiconductors,” *Physica Scripta*, vol. 38, no. 3, pp. 491–497, 1988.

[36] K. M. Gektidis, A. I. Ioannidis, and T. E. Tsovilis, “Response time of surge protective devices employing spark gap technology,” in *Proc. IEEE Ind. Appl. Soc. Annu. Meeting*, 2022, pp. 1–9.

[37] M. Darveniza, “The generalized integration method for predicting impulse volt-time characteristics for non-standard wave shapes - a theoretical basis,” *IEEE Trans. Elect. Insul.*, vol. 23, no. 3, pp. 373–381, Jun. 1988.

[38] Z. G. Datsios, P. N. Mikropoulos, and T. E. Tsovilis, “Insulator string flashover modelling with the aid of an ATPDraw object,” in *Proc. IEEE 46th Int. Universities’ Power Eng. Conf.*, 2011, pp. 1–5.

[39] P. Chowdhuri, A. K. Mishra, and B. W. McConnell, “Volt-time characteristics of short air gaps under nonstandard lightning voltage waves,” *IEEE Trans. Power Del.*, vol. 12, no. 1, pp. 470–476, Jan. 1997.

[40] M. Berger, J.-P. M. Grave, C. Lavertu, I. Kocar, J. Mahseredjian, and D. Ferrara, “Modeling, simulation, and testing of switching surge transients in rapid transit vehicles DC Power Systems,” *IEEE Trans. Ind. Appl.*, vol. 54, no. 1, pp. 822–831, Jan./Feb. 2018.

[41] CIGRE Working Group C4.408, *Lightning protection of low-voltage networks*, Technical Brochure 550, Aug. 2013. [Online]. Available: https://e-cigre.org/publication/550-lightning-protection-of-low-voltage-networks

[42] L. Cheng et al., “Experimental study on the short-circuit failure mechanism of cumulative discharge in gas discharge tube,” *IEEE Trans. Plasma Sci.*, vol. 49, no. 9, pp. 2831–2838, Sep. 2021.

[43] I. Kim, T. Funabashi, H. Sasaki, T. Hagiwara, and M. Kobayashi, “Study of ZnO arrester model for steep front wave,” *IEEE Trans. Power Del.*, vol. 11, no. 2, pp. 834–841, Apr. 1996.

[44] H. Chen and Y.-p. Du, “A comprehensive study on the nonlinear behavior of metal oxide varistors,” in *Proc. IEEE 33rd Int. Conf. Lightning Protection*, 2016, pp. 1–5.

[45] E. T. Staikos and T. E. Tsovilis, “Low-frequency response of low-voltage metal-oxide varistors used for telecommunication systems protection,” in *Proc. IEEE Int. Conf. High Voltage Eng. Appl.*, 2020, pp. 1–4.

[46] J. He, *Metal Oxide Varistors: From Microstructure to Macro-Characteristics*. Hoboken, NJ, USA: Wiley, 2019.

[47] H. K. Høidalen, L. Prikler, and F. Penaloza, *ATPDraw Version 7.3 for Windows Users’ Manual*. Trondheim, Norway: NTNU, 2021.

[48] C. D. Pham, V. Crevenat, and Y. Gannac, “Empirical model of the impulse voltage-time characteristic of gas discharge tube,” in *Proc. 35th Int. Conf. Lightning Protection*, 2021, pp. 1–6.

[49] “Electromagnetic pulse (EMP) protection and resilience guidelines for critical infrastructure and equipment,” National Coordinating Center for Communications (NCC), National Cybersecurity and Communications Integration Center Arlington, Virginia, USA, Feb. 2019, Unclassified. [Online]. Available: https://www.cisa.gov/sites/default/files/publications/19_0307_CISA_EMP-Protection-Resilience-Guidelines.pdf

[50] EPCOS Databook, 2018, Accessed: May 2023. [Online]. Available: https://www.tdk-electronics.tdk.com/download/531268/8954d4a78154a9da5c70a7119fa03e86/siov-general.pdf

[51] G. Furst, *Models Primer*, 1st ed. Montreal, QC, Canada: Can./Amer. EMTP User Group, 1996, pp. 1–60.

Thomas E. Tsovilis (Senior Member, IEEE) was born in Piraeus, Greece, in 1983. He received the M.Eng. and Ph.D. degrees in electrical and computer engineering from the Aristotle University of Thessaloniki (AUTh), Thessaloniki, Greece, in 2005 and 2010, respectively.

He held various managerial positions with the R&D Department of Raycap Corporation, leading innovation in surge protective devices. He was the Director of the High Current Labs of Raycap, Drama, Greece, from 2012 to 2015, and in Ljubljana, Slovenia, from 2016 to 2018. In 2018, he joined AUTh, where he is an Associate Professor. He has authored more than 100 scientific papers in his research areas which include the broad area of high voltage engineering with emphasis given to electrical discharges, lightning & surge protection, and insulation coordination for power systems. He is the inventor of eight granted U.S. patents on surge protective devices and testing techniques.

Alexandros Y. Hadjicostas (Graduate Student Member, IEEE) was born in Nicosia, Cyprus, in 1996. He received the M.Eng. degree in electrical and computer engineering from the Aristotle University of Thessaloniki (AUTh), Thessaloniki, Greece, in 2021. He is currently working toward the Ph.D. degree in the High Voltage Laboratory, AUTh.

His research interests include surge protection with emphasis given on EMT modeling and appropriate dimensioning and effective coordination of surge protective devices.

Evangelos Theocharis Staikos (Graduate Student Member, IEEE) was born in Thessaloniki, Greece, in 1994. He received the M.Eng. degree in electrical and computer engineering from the Aristotle University of Thessaloniki (AUTh), Thessaloniki, Greece, in 2018. He is currently working toward the Ph.D. degree with the High Voltage Laboratory, AUTh.

His research interests include metal-oxide varistors characterization and modeling, surge protection of power, telecommunication, and automotive systems.

Georgios D. Peppas (Senior Member, IEEE) was born in Rustenburg, South Africa, in 1987. He received the Diploma degree in electrical engineering and the Ph.D. degree from the Department of Electrical and Computer Engineering, University of Patras, Patras, Greece, in 2011 and 2016, respectively. Since 2016, he has been R&D Manager of Raycap S.A., Drama, Greece, leading innovation in surge protective devices, and Technical Manager of the High Current Laboratory of Raycap S.A., (IECEE CTF Stage 3). Since 2016, he has been collaborating with the High Voltage Laboratories of NTUA, Upatras, and AUTH. He is the author of more than 50 papers in major international peer reviewed scientific journals and conference proceedings, and is an inventor of four patents. His research interests include lightning protection, nanofluids for high voltage applications, insulation coordination of power systems, dielectric liquids, and induced lightning phenomena.